8-2018

Observing the Gamma-Ray Burst–Supernova Connection with 1m-class Aperture Telescopes

Corinne Maly Taylor
Clemson University, corinn4@clemson.edu

Observing the Gamma-Ray Burst–Supernova Connection with 1m-class Aperture Telescopes

---

A Thesis
Presented to
the Graduate School of
Clemson University

In Partial Fulfillment
of the Requirements for the Degree
Master of Science
Physics

---

by
Corinne Maly Taylor
August 2018

Accepted by:
Dr. Dieter Hartmann, Committee Chair
Dr. Máté Ádámkovics
Dr. Joan Marler

Abstract

Observations over the past two decades indicate that some gamma-ray bursts (GRBs) are associated with core-collapse supernovae (SNe). We explore the connection between nature's two biggest explosions by reviewing their photometric properties and standard models. Using three small telescopes (1-m class) belonging to the Southeastern Association for Research in Astronomy (SARA) consortium, we observed four events and present our findings here. These events include a connected GRB-SN (GRB 171205A/SN 2017iuk), an orphan afterglow (AT 2018cow), a burst with a faint afterglow (GRB 180620A), and a burst with no afterglow (GRB 180514). We performed photometric measurements of these events and compared our data with data of other observers. To further explore the GRB-SN connection, we considered cosmological effects such as luminosity distance, time dilation, and K-corrections. These were applied to photometric data of SN 1998bw, the GRB-SN that confirmed the relation between the two phenomena. This template was compared to data of GRB 980326 to determine the burst's redshift, an exercise that has been performed previously in other studies. We also modeled the light curve of SN 2017iuk using the template as well as predicted when a supernova may have emerged from AT 2018cow. We established an upper limit of $R \sim 21$ when observing on SARA, which constrains GRB observations to those at redshifts of $z \leq 0.22$. Lastly, we propose a simple outline for using 1-m class telescopes to observe gamma-ray bursts and supernovae.

Acknowledgments

I would first like to thank my thesis advisor, Dr. Dieter Hartmann, of the Physics and Astronomy Department at Clemson University. He gave me guidance when needed and always helped to steer me in the right direction. I would also like to thank Dr. Amanpreet Kaur for teaching me almost everything I know about remotely observing on telescopes and using IRAF for photometry. Without her, the work for this thesis would have been much more difficult. Finally, I would like to acknowledge my fellow observers at Florida Gulf Coast University, namely Nick Rimbert and Dr. Ken Watanabe, for sharing several of their observing nights with me and even taking data images at times. From them I learned that advancement of science truly is a collaborative effort. Thank you.

Table of Contents

List of Tables

List of Figures

Chapter 1

Introduction

Gamma-ray bursts (GRBs), first observed in the late 1960s by the Vela satellites (Klebesadel et al. 1973), are intense flashes of electromagnetic radiation that last on the order of seconds and have typical photon energies of several hundred keV. These bursts arrive at Earth from unpredictable locations and can occur several times each day. Early theories predicted that the source of GRBs was local, created within the Milky Way galaxy. However, data from the Burst and Transient Source Experiment (BATSE) aboard the Compton Gamma-Ray Observatory (CGRO) showed that GRBs are isotropically distributed across the sky, thereby providing evidence that the bursts are of extragalactic origin (Fishman & Meegan 1995).

Because light curves of gamma-ray bursts are complex and diverse, there have been many (often failed) attempts to classify the bursts based on similar spectral, spatial, or morphological properties. However, a plot of GRB durations shows a bimodal distribution with a minimum around 2.0 seconds (Kouveliotou et al. 1993), where durations are defined by T_{90}, or the time to accumulate between 5% and 95% of the total photon counts (see Figure 1.1). This bimodality suggests two classes of gamma-ray bursts: the "short" bursts and the "long" bursts, which respectively have mean durations of 0.33 seconds and 26.2 seconds. The light curves of long bursts often have multiple peaks of short, overlapping pulses with peak energies of 220 keV, whereas short bursts tend to be very intense and

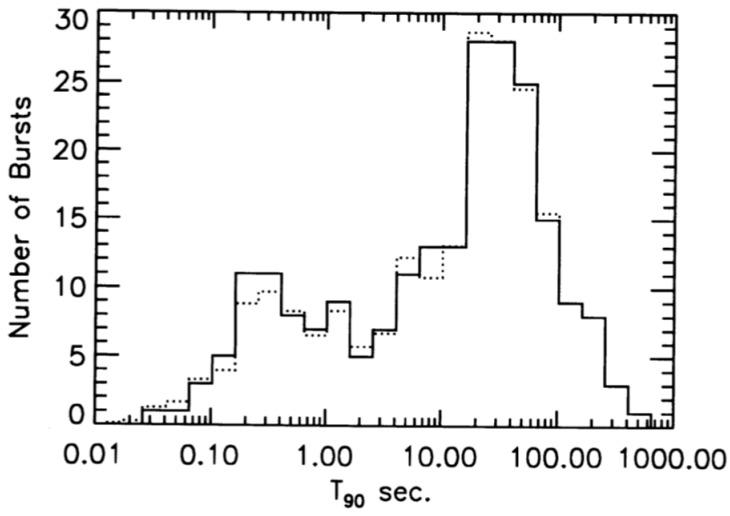

Figure 1.1: Histogram of gamma-ray burst durations, defined by T_{90}. The bimodality of the plot indicates two classes of bursts. From Kouveliotou et al. (1993).

symmetric with peak energies of 360 keV (Hakkila et al. 2000).

With the classification of long and short bursts came several various theories to explain their progenitors. Precise and rapid localizations of short bursts indicated an association with regions of little or no star formation, such as elliptical galaxies (Bloom et al. 2006). This ruled out massive stars as a source of short bursts and provided support towards the leading hypothesis that they instead originate from neutron star-neutron star mergers or neutron star-black hole mergers (Bloom et al. 2006). Confirmation for this theory came with the detection of short GRB 170817A only 1.7 seconds after the detection of gravitational wave GW170817, a signal from the merger of two neutron stars located about 40 Mpc away (LIGO Scientific Collaboration et al. 2017). A transient observed across the ultraviolet, optical, and infrared wavelengths (known as a *kilonova*) provided further identification of the host galaxy.

Most observed gamma-ray bursts ($\sim$70%) are of the long type. These long GRBs have been studied more intensively than their short counterparts. The localization of their afterglows indicated an association with young, active star-forming galaxies and an origin of massive star death (Woosley & Bloom 2006). The connection between supernovae (SNe)

and gamma-ray bursts was evidenced by the discovery of a burst on April 25, 1998 (GRB 980425), which was coincident in both time and place with a bright core-collapse supernova, SN 1998bw (Galama et al. 1998). Spectroscopic identification of supernova features occurring after the GRB event firmly established a physical link between the two (Hjorth & Bloom 2012). Since then dozens of connections have been proposed between GRBs and SNe, and the list is continuously growing. These GRB-SNe are included in Table 1.1.

In Chapter 2 we further examine the GRB-SN connection by exploring their characteristics and the standard model. We also consider SN 1998bw to be "the template" for all long GRBs arising from core-collapse supernovae. In Chapter 3 we introduce the basics of photometry and photometric systems, with further discussion in Appendix A. In Chapter 4 we present our own data from observations of SN afterglows, taken with the Southeastern Association for Research in Astronomy (SARA) 1-meter class telescopes. Our data is supplemented with data from other literature. Chapter 5 focuses on cosmological modeling of SN 1998bw to recreate Figure 1 of Bloom et al. (1999), in which we consider luminosity distance, K-corrections, and time dilation of GRB 980326. We apply our SN 1998bw template to data of recent events observed with the SARA telescopes in Chapter 6. Finally, we discuss and conclude in Chapter 7 and urge other observers on small telescopes to also chase GRBs and SNe.

GRB	SN	z	T_{90} (s)	m_{peak}	Reference
920613	1992ae	0.075	129.4	18.47_V	IAUC5554
951107	1995bc	0.048	43.52	18.5_V	IAUC6275
970514	1997cy	0.063	1.3	16.8	IAUC6706
980425	1998bw	0.0085	18	13.6	IAUC6895
991002	1999eb	0.018	1.9	16.2	IAUC7268
011121	2001ke	0.362	47	23.0	IAUC7857
020211	2002lt	1.006	2.80	24.5	IAUC8197
030329	2003dh	0.1685	22.76	16.2	IAUC8114
031203	2003lw	0.1055	37.0	20.5	IAUC8308
050525A	2005nc	0.606	8.84	24.0	IAUC8696
060218	2006aj	0.0334	2100	17.3	IAUC8674
081007	2008hw	0.53	9.01	16.4	CBET1602
091127	2009nz	0.49	7.42	21.6	CBET2288
100316D	2010bh	0.0591	1300	20.0	CBET2227
101219B	2010ma	0.552	51	17.8	CBET2706
111209A	2011kl	0.67702	10000	20.0	CBET4196
120422A	2012bz	0.2383	5.35	20.6	CBET3100
120714B	2012eb	0.3984	159	18.6	CBET3200
130215A	2013ez	0.597	40	14.2	CBET3637
130427A	2013cq	0.3399	162.8	12.0	CBET3531
130702A	2013dx	0.145	59	17.4	CBET3587
130831A	2013fu	0.4791	32.5	14.1	CBET3677
161219B	2016jca	0.1475	6.94	19.0	GCN20308
171010A	2017htp	0.328	70.3	21.8	GCN21985
171205A	2017iuk	0.037	189.4	16.0	GCN22177

Table 1.1: Gamma-ray bursts with associated supernovae. Magnitudes are reported for the R band unless noted by a subscript. Data from Guessoum et al. (2017), Hjorth & Bloom (2012), Modjaz et al. (2016).

Chapter 2

The GRB-SN Connection

Colgate (1968) first proposed a model of gamma-ray bursts before the phenomenon had even been discovered, associating them with the breakout of shocks from the surfaces of supernovae. However, the discoverers of such gamma-ray emissions found no evidence for the predicted connection with SNe (Klebesadel et al. 1973). For over two decades, thousands of GRBs and hundreds of SNe were localized and yet no connection was established. By 1997, the search for GRB counterparts came to fruition with the first rapidly available and accurate GRB error boxes, produced by the two Wide Field Cameras (WFC) on the *BeppoSAX* satellite (Boella et al. 1997). Follow-ups of bursts eventually pointed towards a cosmological origin, occurring in regions of active star formation. Paczynski (1986) predicted that these "gamma-ray bursters" would release 10^{51} ergs within 1 second, making them comparable to the kinetic energy released by a supernova. As redshifts of GRBs were determined and geometric corrections made to account for beaming, the total energy release in γ-rays was found to be around 10^{51} ergs, as had been hypothesized (e.g. Kumar & Piran (2000)).

Despite this similarity in energy between GRBs and SNe, the phenomena were considered unrelated. The event that clicked the connection into place was the discovery of GRB 980425, which occurred on April 25, 1998. This underluminous GRB was coincident in time (within a few days) and location (within a few arcminutes) with SN 1998bw, an

unusually bright supernova ($E_K = 10^{52}$ ergs; Galama et al. (1998)) located in the late-type galaxy ESO184-G82 at a redshift $z = 0.0085$ (Tinney et al. 1998). Although the connection was initially doubted by some, X-ray data confirmed the association of the GRB with the supernova (Pian et al. 2000). Spectroscopic analysis of SN 1998bw revealed a lack of H and He absorption lines with a weak Si II absorption line, suggesting a classification of a Type Ic broad-line supernova (Patat & Piemonte 1998). However, at such a low redshift, the energy emitted in gamma-rays was calculated to be $E_\gamma = 8.5 \pm 0.1 \times 10^{47}$ ergs, over three orders of magnitude fainter than what is expected of long-duration bursts (Woosley & Bloom 2006). In addition, no optical afterglow was detected, as is common in most other GRBs (see Section 2.1). These three factors caused some (e.g., Kulkarni et al. (1998)) to point towards a different class of GRB than the "truly cosmological GRB", defined by a significant redshift, high energy output, and an afterglow decaying as a power-law (Hjorth & Bloom 2012).

Nevertheless, SN 1998bw was thoroughly observed and its light curve was the subject of many extensive studies (e.g. Clocchiatti et al. (2011), Patat et al. (2001), Sollerman et al. (2002)). With spectral and photometric data readily available (see Figure 2.1), SN 1998bw is often used as a template to constrain other supernova light curves. For a typical GRB-SN, the three components of measured flux are the afterglow (AG), the supernova, and the host galaxy's constant source. In order for the SN component to be analyzed, it must first be decomposed from the optical light curve. The late-time "supernova bump" is then compared to a template supernova, namely SN 1998bw. This approach has been used in many studies (e.g. Cano et al. (2014), Cano et al. (2017), Zeh et al. (2004)), pointing towards SN 1998bw as "the template" for all GRB-SNe.

Almost five years later, on March 29, 2003, any doubts were eliminated concerning the connection between gamma-ray bursts and supernovae with the detection of GRB 030329 in accordance with SN 2003dh. At a redshift of $z = 0.1685$ (Greiner et al. 2003), the burst was considered truly cosmological and, unlike GRB 980425, was followed by a very bright afterglow ($R \sim 13$; Price & Peterson (2003)). The optical spectrum of the burst

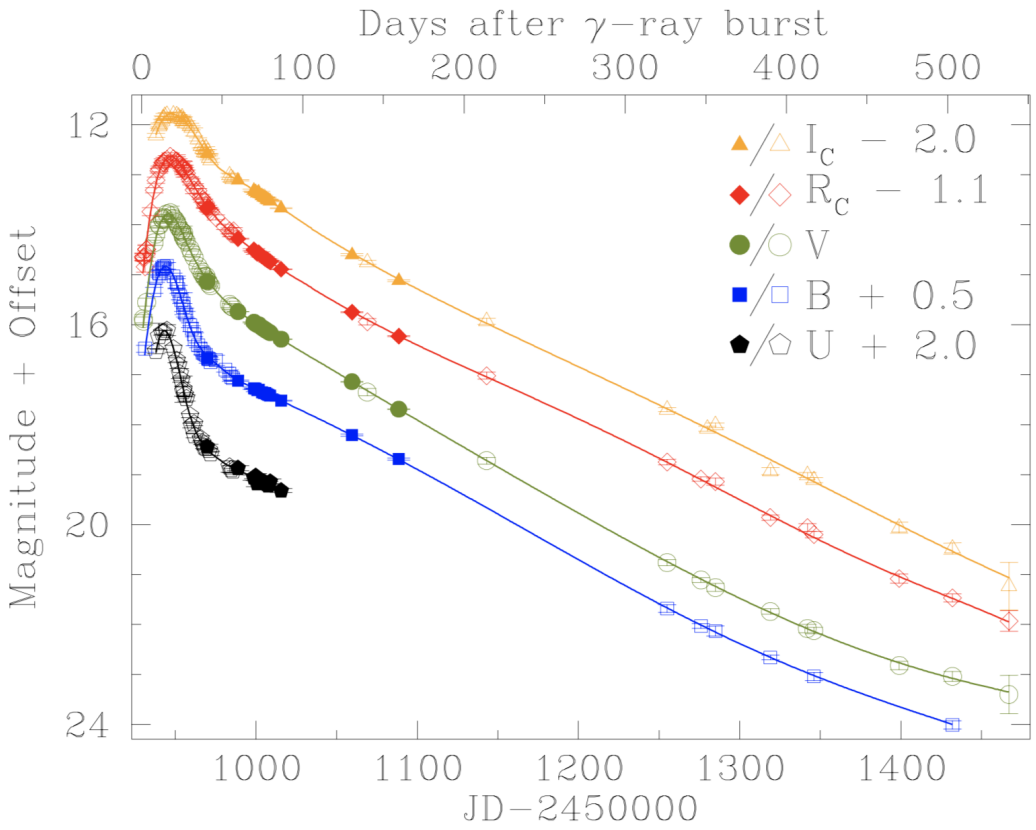

Figure 2.1: Complete light curves of SN 1998bw. Open symbols display the earlier observations of Galama et al. (1998) and later observations of Sollerman et al. (2002). Solid symbols bridging the two sets are observations presented by Clocchiatti et al. (2011). From Clocchiatti et al. (2011).

faded following a featureless power-law spectrum ($F \propto t^{-\alpha}$), and broad SN spectral features emerged several days later (Hjorth et al. 2003). This SN spectrum closely followed that of SN 1998bw, although SN 2003dh evolved faster (see Figure 2.2; Hjorth et al. (2003)). The connection between GRB 030329 and SN 2003dh in turn provided evidence towards the association of GRB 980425 with SN 1998bw.

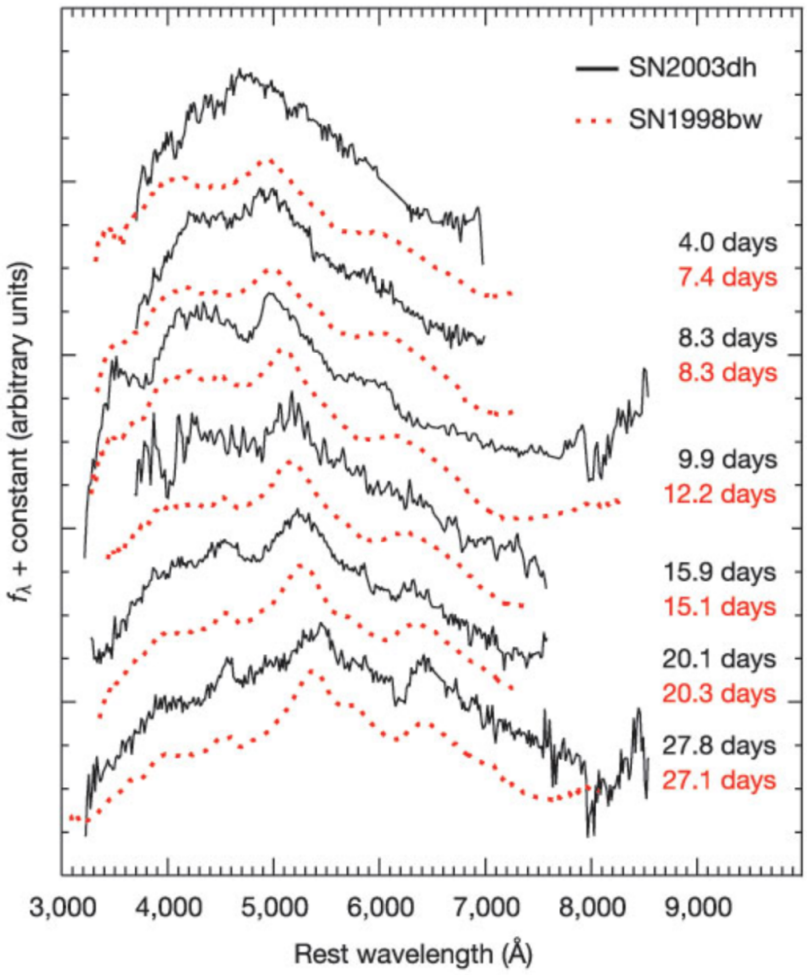

Figure 2.2: Spectral evolution of GRB-SNe 1998bw (Patat et al. 2001) and 2003dh (Hjorth et al. 2003). Solid lines indicate the spectra of SN 2003dh and dotted lines indicate spectra of SN 1998bw. Times are indicated in the rest frame, days after the GRB. From Hjorth et al. (2003).

2.1 Characteristics of GRB-SNe

Supernovae associated with long-duration gamma-ray bursts differ from all other SNe in several ways. Perhaps one of the most notable differences is the significant amount of kinetic energy that is concentrated into relativistic ejecta (Woosley & Bloom 2006). In order to produce a GRB, the energy in the relativistic ejecta must be at least that of the energy that is observed in γ-rays and afterglow emission ($E_{Rel} \geq E_\gamma$). Because of the

effects of beaming, the value of E_γ can be difficult to measure directly but is estimated to be around 10^{51} ergs (Bloom et al. 2003). E_{Rel}, inferred from late-time radio observations, is measured to be $\sim 5 \times 10^{51}$ ergs.

GRB-SNe are most likely Type Ic-BL SNe, based on the spectroscopic data of various GRB-SNe. These supernovae have an absence of hydrogen in their spectra, placing them in the Type I classification. Sufficient spectra observations also indicate an absence of neutral helium (He I) and weak or absent absorption lines of singly-ionized silicon (Si II), leading to a Type Ic classification. Broad-line (BL) features are also apparent in the spectra of GRB-SNe; these features are due to high velocities, such as the Si II line width of SN 1998bw that suggested expansion speeds of 30,000 km s^{-1} (Patat et al. 2001). The differences in spectral features of various types of supernovae are shown in Figure 2.3 (Modjaz et al. 2014).

Because of the brightness of GRB-SNe, theory demands a high production of ^{56}Ni to power the luminosity for long timescales (weeks to months). The combination of high mass, high velocity, and high ^{56}Ni mass implies a kinetic energy of $E_{SN} \sim 10^{52}$ ergs (Woosley & Bloom 2006). In order for the iron core to collapse into a neutron star or black hole, energy must be released on the order of $E_\nu \sim 10^{53}$ ergs. From this explosion, 99% is carried by neutrinos, 1% goes into kinetic energy of the expanding ejecta, and 0.01% goes into light; the energy of the ejecta is then $E_K \sim 10^{51}$ ergs (Hartmann 2010).

As the most energetic explosions in the universe, it may seem surprising that a connection between GRBs and SNe took several years to establish. However, the rate for GRB-SNe is not as frequent as one may expect. The supernova rate is estimated as 1 SN/100 yrs/1 Milky Way-type galaxy or ~ 0.5 Gpc^{-3} yr^{-1} (Schmidt 2001). An estimated $15 - 20\%$ of all SNe are observed to be of Type Ib/c, or $\sim 4.8 \times 10^4$ Gpc^{-3} yr^{-1} (Marzke et al. 1998). Of all Type Ib/c SNe, about $5 - 10\%$ are classified as SN Ic-BL; this indicates a rate of about $10^{-6} - 10^{-5}$ per year. At the 90% confidence level, less than 10% of all SN Ib/c have an off-axis GRB (Soderberg et al. 2006).

The data thus indicate that most long GRBs do not have a detected associated supernova. Regardless, some favor the hypothesis that all long-duration GRBs lead to

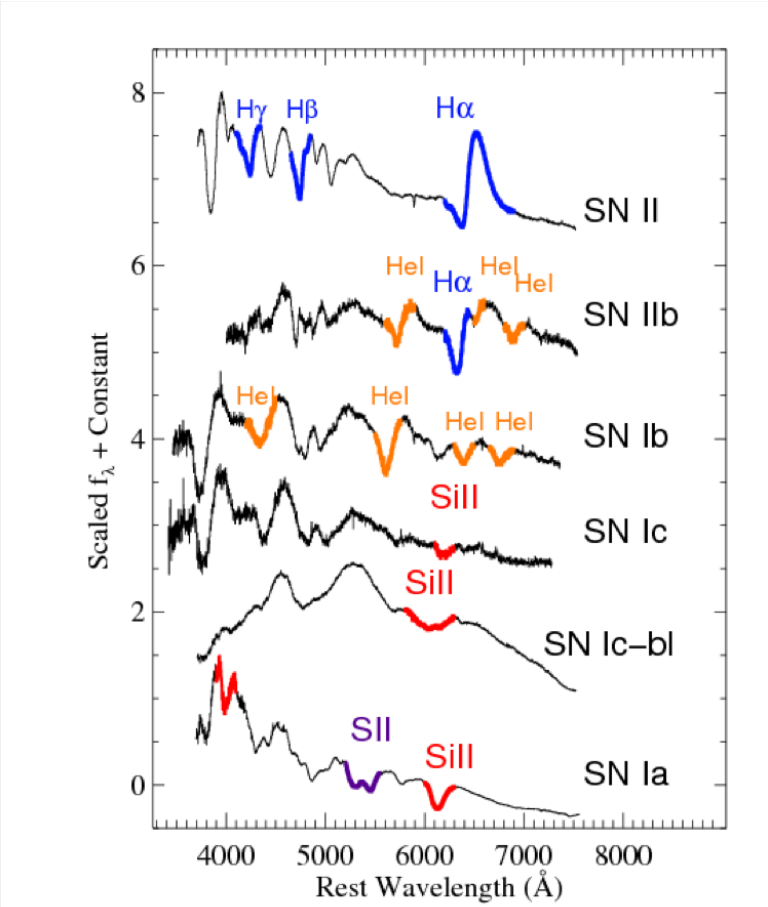

Figure 2.3: Montage of the main supernova types, in order to highlight the distinguishing features of their spectra. These main distinguishing features are marked in color and annotated. From Modjaz et al. (2014).

supernovae (e.g. Bloom et al. (2003)) and extrinsic biases result in a decreased probability of detecting a supernova. We note that many of the connected GRB-SN events occur within redshift $z < 0.5$ (see Figure 2.4), most likely due to the biases briefly listed here (Woosley & Bloom 2006):

1. *Localization* - Poor localization of bursts impede the ability of telescopes to discover emerging supernovae.

2. *Dust* - The sensitivity of SN observations may be diminished, particularly for those that occur near the line-of-sight through the galaxy.

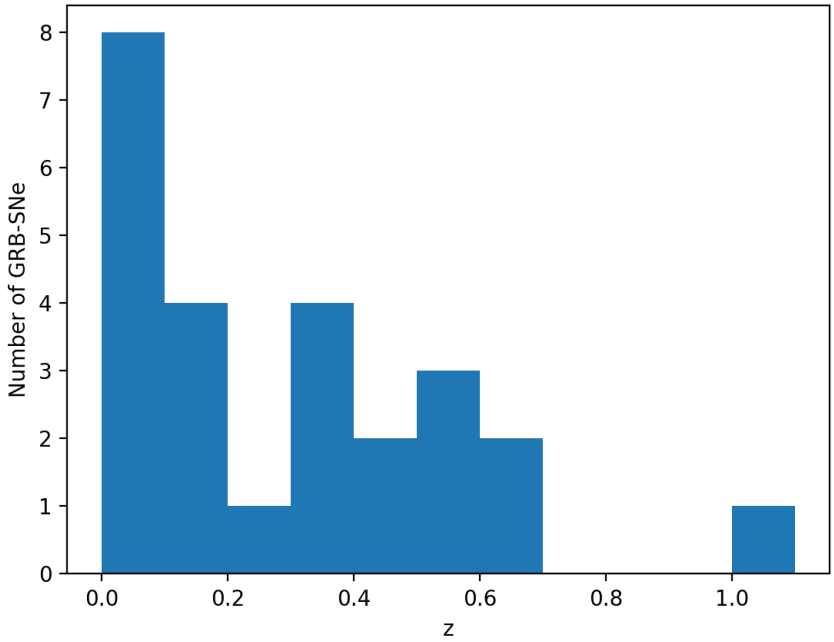

Figure 2.4: Number of GRB-SNe at redshifts to $z \approx 1$. Data from Table 1.1.

3. *Redshift and luminosity distance* - Higher redshifts ($z \approx 0.5$) imply high K-corrections and higher distance modulus and a greater suppression of emissivity, making Type Ib/c SNe more difficult to detect.

4. *Host galaxies* - The host galaxies of GRBs may contaminate the light of SN such that resolving out diffuse host light may become impossible.

2.2 The Collapsar Model

Various models of ordinary core-collapse supernovae have been explored in the literature (e.g. see sources contained within Woosley & Bloom (2006)). The "standard model" of the *collapsar* (e.g. MacFayden et al. (2001)) begins with a main-sequence massive star ($M > 30M_{\odot}$). At $T \sim 10^{10}$ K and $\rho \sim 10^{10}$ g cm^{-3}, the iron core of the star collapses, triggered by electron capture and photodisintegration. A rebound launches a shock wave but

quickly loses velocity due to neutrino loss. Much of the ejected mass falls back onto the core remnant at a rate of $0.1 - 0.3\,M_{\odot}/\mathrm{s}$, producing a black hole or a "proto-neutron star". If the star is rotating quickly enough, the gravitational potential energy of the infalling material drives a pair of relativistic jets out along the rotational axis. These jets transfer enough energy into the ejected shell that a superluminous supernova can be observed. Gamma-rays are geometrically beamed outwards by the jets to angles of $\sim 5^{\circ} (\sim 0.1$ rad), meaning that observers will not detect the jets if they are outside the viewing angle. Supernovae, on the contrary, emit isotropically and therefore can be viewed from any angle.

With this collapsar model comes a few constraints (Woosley & Heger 2006). First, the star undergoing core-collapse must be massive enough to produce a neutron star or a black hole with enough explosion energy to expel the outer layers of the star; this places a lower limit of around 10 $M_{\odot}$. If the star is too massive, however, a black hole may form before an outgoing shock is launched. Second, the star must be rapidly rotating in order to develop an accretion torus and drive the jets outwards after collapse; too little rotation will fail to create a gamma-ray burst. Third, the star must have low metallicity and must lose its hydrogen envelope prior to collapse. Stars with low metallicity tend to have a lower mass loss rate; too much mass loss makes the star too light to explode into a black hole (Woosley & Bloom 2006).

Chapter 3

Photometric Observations of Afterglows

In order to observe the evolution of gamma-ray bursts and supernovae, photometric measurements must be taken. Photometry, derived from the Greek *photos* ("light") and *metron* ("measure"), is the measure of flux of an object's electromagnetic radiation (Sterken & Manfroid 1992). For astronomical purposes a charged-coupled device (CCD) is often used to observe and record these signals in terms of counts and convert the counts into instrumental magnitudes. The instrumental magnitudes are compared to known magnitudes of other objects, such as *standard stars*, in order to determine the magnitudes of the observed objects. In this chapter we present a brief overview of photometry, as the topic is rather extensive and can fill entire books (e.g. Sterken & Manfroid (1992); Kitchin (1998); Howell (2000)). More in-depth information is described in Appendix A.

3.1 Basics of Photometry

To begin photometry, the proper calibration images–bias frames, dark frames, and flat frames–must be taken and correctly applied to the data images, which consist of both the object frames and the frames containing a set of Landolt standard stars. The magnitudes of

these standard stars (Landolt 1992) have been thoroughly studied and measured, allowing them to be used as a comparison for the magnitudes of other celestial objects. This method of comparing instrumental magnitudes to stars of known magnitudes is known as *relative photometry*. The Landolt standard stars are centered around the celestial equator so they can be observed from either hemisphere; they are also non-variable, not too bright as to saturate detectors ($11.5 \leq M \leq 16.0$), and individual sets are close together and cover a wide color range (-0.3 to $+2.3$).

After the data images have been reduced, photometric measurements can be made. Image processing programs such as IRAF (Interactive Reduction and Analysis Facility), IDL (Interactive Data Language), or ESO-MIDAS (European Southern Observatory - Munich Image Data Analysis System) are used to convert the count rates measured by the CCD into instrumental magnitudes. After atmospheric extinction corrections and comparisons to standard stars, these instrumental magnitudes are converted into magnitudes that can be placed on a standard physical flux scale. In this study we used IRAF to reduce our data and take photometric measurements.

3.2 Photometric Systems

The total luminosity of an object, integrated over all wavelengths, is known as its *bolometric luminosity*. However, observing celestial objects over all wavelengths is often not necessary or even possible. Filters are often used to pass through only certain wavelengths of light. Various photometric systems, which are defined by a list of standard magnitudes and colors measured at specific bandpasses, are used to determine the magnitudes of objects (Bessell 2005). These systems have a known sensitivity to incident radiation and are characterized according to the widths of their passbands. For example, broad band systems have passbands wider than 400 Å, such as the Johnson-Cousins $UBVRI$ system that is used in this study. Figure A.1 shows the transmission windows of the $UBVRI$ filters and Table A.1 shows the peak wavelengths and widths of the system.

In general, an object such as a star has a different magnitude depending on the filter used to observe it. The magnitude of an object is defined as

$$m_R = -2.5\log_{10}(\mathrm{F_R}) + \mathrm{ZP}, \tag{3.1}$$

where the subscript R indicates that the object was observed through the R passband. The added constant ZP sets the zero-point of the magnitude scale in use. The STMag system uses the flux density of Vega at the effective wavelength of the Johnson V band ($\sim$ 5500 Å) to set the zero point (Phillips 2008), leading to the relation

$$m_\lambda = -2.5\log_{10}(\mathrm{F}_\lambda) - 21.1. \tag{3.2}$$

This indicates that we can determine a star's magnitude if we know its flux at a certain wavelength. If two stars are observed through the same filter, the difference between their magnitudes can be determined using the relation

$$m_1 - m_2 = -2.5\log_{10}(\mathrm{F_1/F_2}), \tag{3.3}$$

where F_1 and F_2 are the fluxes of each star. In addition to the passband used, observed light from an object can be diminished by Earth's atmosphere. A star at the zenith will suffer the least from *atmospheric extinction*, whereas a star closer to the horizon will suffer the most, as the path length through the atmosphere is longer (Bessell 2005). This path length is called the *airmass*, approximated by $\sec(Z)$ such that the airmass is 1 at zenith. Both the airmass and the passband used must be taken into consideration when determining photometric values.

Even after considering the filter, airmass, and exposure time (among many other variables), observers are nevertheless limited by the upper limits of the telescope used. Small telescopes, often around 1 meter in diameter, are only able to detect objects up to $\sim$20th magnitude. Larger telescopes, such as the 10-m Keck Telescope, have an upper limit

of almost 26th magnitude (Keck Observatory 2016). Even more advantageous, telescopes above the Earth's atmosphere avoid sky brightness and can see even deeper objects; the James Webb Space Telescope (JWST) is expected to have an upper limit of 34th magnitude (Mather 2017). Knowing the upper limit of a telescope allows observers to smartly choose targets for photometric or spectroscopic studies.

Chapter 4

Observations with SARA

The Southeastern Association for Research in Astronomy (SARA) is a consortium consisting of over ten southeastern colleges and universities with small astronomy departments (Keel et al. 2016). Members include Clemson University, University of Alabama, Florida Gulf Coast University, and Butler University, among others. The consortium operates three telescopes in various locations: the 0.96 m telescope at Kitt Peak, Arizona (SARA-KP), a 0.6 m aperture on Cerro Tololo, Chile (SARA-CT), and the 1.0 m Jacobus Kapteyn Telescope at the Roque de los Muchachos, La Palma, Spain (SARA-RM). Each telescope has a CCD system and is controlled remotely.

Use of all three SARA telescopes has been vital to this study for observing gamma-ray burst afterglows and supernovae. Some of the data has been supplemented with data from the Gamma-ray Coordinates Network (GCN) and/or The Astronomer's Telegram (ATel). We report our observational data for several events in the following sections.

4.1 GRB 171205A / SN 2017iuk

Swift detected a burst at 07:20:43 UT on December 5, 2017 located at a right ascension of 11:09:47 and a declination of -12:36:12 (D'Elia et al. 2017). The XRT position contained the spiral galaxy 2MASX J11093966-1235116, located at $z = 0.037$ (Izzo et al.

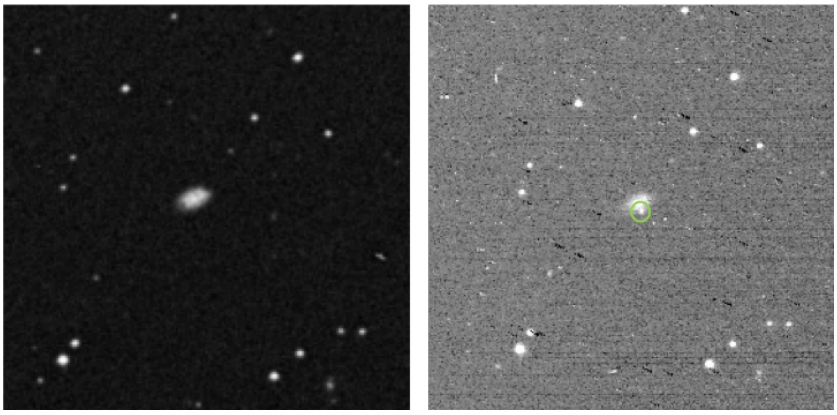

Figure 4.1: Finding chart of SN 2017iuk. The left image is an archival DSS image and the right image is a stacked R-band image taken with SARA-CT.

Site	Date (UT)	R	V	B
RM	2017-12-09 06:17	18.485 ± 0.075	18.913 ± 0.053	17.789 ± 0.093
CT	2017-12-15 07:11	17.729 ± 0.020	17.779 ± 0.022	18.753 ± 0.045
CT	2017-12-21 07:26	18.140 ± 0.016	17.832 ± 0.023	19.159 ± 0.070
CT	2017-12-28 04:47	17.966 ± 0.020	17.697 ± 0.069	18.962 ± 0.066
KP	2017-12-31 11:44	18.044 ± 0.021	18.274 ± 0.036	–

Table 4.1: Photometric values for GRB 171205A/SN 2017iuk in the R, V, and B filters. Data was taken using the SARA telescopes in December 2017.

2017a); spectroscopic observations confirmed this redshift and an optical afterglow was detected (Izzo et al. 2017b), following a power-law decay with index $\alpha = 1.41 \pm 0.14$ (Barthelmy et al. 2017). Spectral features were similar to the early spectra of SN 1998bw, indicating that GRB 171205A had a broad-lined Ic supernova counterpart, SN 2017iuk (de Ugarte Postigo et al. 2017). We observed this GRB-SN for five nights using the SARA telescopes and found photometric values for the B, V, and R bands (see Table 4.1). We combined our R-magnitude data points with R-magnitude data from GCNs to create Figure 4.2.

4.2 AT 2018cow

ATLAS detected a bright transient source on June 16, 2018 at 10:35:02 UT at a right ascension of 16:16:00.22 and a declination of +22:16:04.8 (Smartt et al. 2018). The source

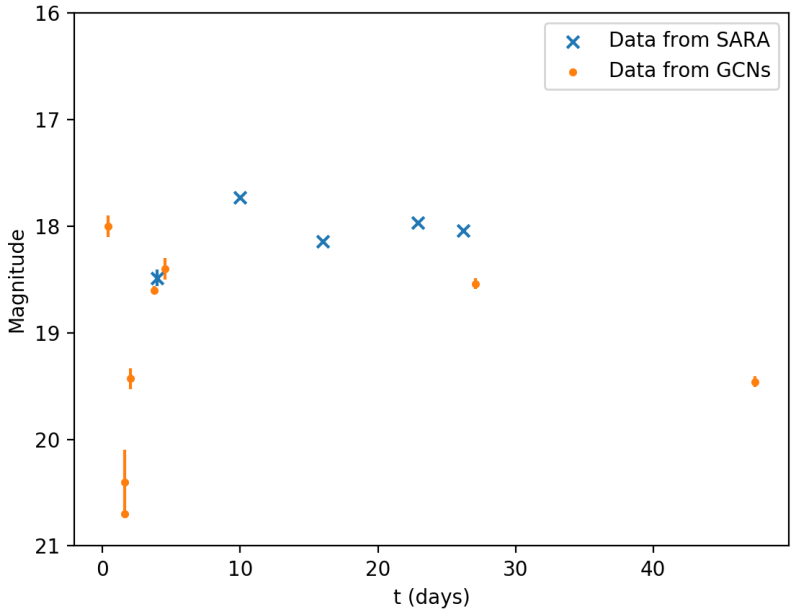

Figure 4.2: R-magnitude data of GRB 171205A / SN 2017iuk. Blue x's indicate data taken using the SARA telescopes and orange dots indicate data taken from GCNs. Time in days indicates the time since the detection of GRB 171205A.

is spatially coincident with the galaxy CGCC 137-068, which is at a redshift $z = 0.014145$, and was thought to be a cataclysmic variable, a bright supernova, or something else. The host galaxy has a magnitude of 15.7 (Zwicky & Herzog 1963). Spectroscopy of the transient revealed a mostly featureless spectrum and a weak broad-lined feature at ~ 5040 Å, similar to a feature found in Ic-BL SN spectra (Rivera Sandoval & Maccarone 2018); this led some observers to believe that the "orphan afterglow" may be the supernova counterpart to an off-axis GRB. We observed this transient for four nights using the SARA-KP and SARA-RM telescopes and found photometric values for the R band (see Table 4.2). We combined our R-magnitude data with R-magnitude data from ATels to create Figure 4.4; we also include a magnitude taken on SARA-RM by a fellow member of the consortium, Bill Keel of University of Alabama. However, we note that our magnitudes on 2018-06-21 and 2018-06-22 are about half a magnitude brighter than those announced in Astronomer's

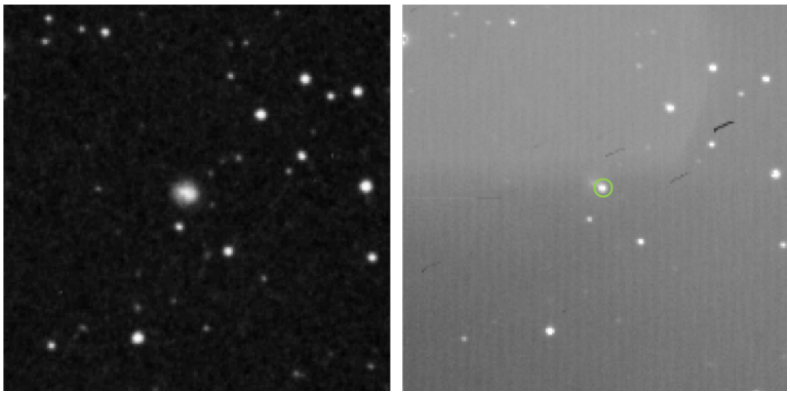

Figure 4.3: Finding chart of AT 2018cow. The left image is an archival DSS image and the right image is a stacked R-band image taken with SARA-KP.

Site	Date (UT)	R
KP	2018-06-20 05:28	14.266 ± 0.010
KP	2018-06-21 03:50	14.035 ± 0.007
KP	2018-06-22 03:37	14.170 ± 0.014
RM	2018-07-06 01:06	15.030 ± 0.010
RM	2018-07-17 21:36	15.473 ± 0.019

Table 4.2: Photometric values for AT 2018cow in the R filter. Data was taken using the SARA-KP and SARA-RM telescopes in June and July 2018.

Telegrams; this could be due to photometric techniques that did not completely subtract the background light of the host galaxy.

4.3 Other Observations

As described in Chapter 2, not all gamma-ray bursts appear to have an associated supernova. Some supernovae are also too faint to observe using the SARA telescopes due to their upper limits of ∼20th magnitude. In this section, we present data for two bursts that we observed but had no associated supernovae.

4.3.1 GRB 180514

Swift detected a burst on May 14, 2018 at 13:25:33 UT with a right ascension of 13:09:36 and a declination of +36:58:10 (LaPorte et al. 2018). Follow-up observations could

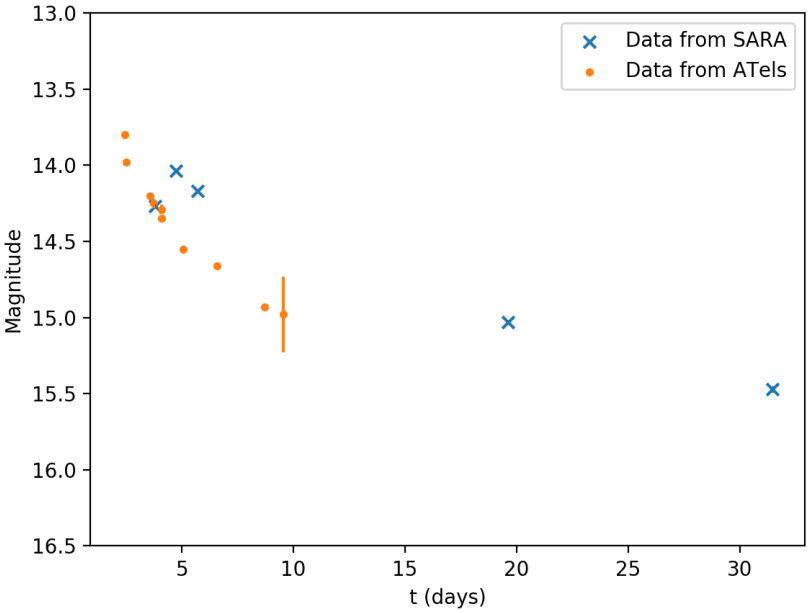

Figure 4.4: R-magnitude data of AT 2018cow. Blue x's indicate data taken using the SARA-KP telescope and orange dots indicate data taken from ATels. Time in days indicates the time since the detection of the transient source.

not detect a credible afterglow candidate. We observed the position of the burst on 2018-05-17 and 2018-05-22 using SARA-RM but also did not detect an afterglow. Using this data we were able to obtain an upper limit of 20.63 for the R-band magnitude, a value that is lower than the limiting magnitude given for the SARA-RM telescope (see Table B.3).

4.3.2 GRB 180620A

Swift detected a burst located at right ascension 18:39:32 and declination +23:15:55 on June 20, 2018 at 08:34:58 UT (Evans et al. 2018). A candidate afterglow was detected nearby with a R-band magnitude of 18.63 (Guidorzi et al. 2018), but the afterglow faded quickly to a magnitude ∼23 within 20 hours after the GRB trigger (Schweyer & Schady 2018). We observed the position of the burst at 04:34 UT on June 21, 2018 but did not see the afterglow as it was too faint to detect with SARA-KP. The magnitude obtained from

photometry of a star located close to the burst is similar to the magnitude that is given by the USNO-A2.0 catalogue; we obtained a magnitude of 16.92 ± 0.03 whereas the accepted magnitude is 16.40 (Monet et al. 1997).

Chapter 5

Cosmological Modeling

Because SN 1998bw was a close, bright supernova, it was thoroughly observed and analyzed. Although GRB 980425 did not have an optical afterglow, this GRB-SN can be used as a template for other GRB-SNe. Oftentimes the distance to a supernova is unknown because of a lack of spectroscopic observations; using the light curve of SN 1998bw as a template can provide constraints on supernova distance as well as a predicted peak time and duration. The template need only be translated and stretched to match the light curves of other supernovae in question.

For example, GRB 980326 was detected on March 26, 1998 by BeppoSAX and an optical afterglow was identified (Groot et al. 1998). A power-law decay is apparent in the light curve as is a subsequent rebrightening phase (Bloom et al. 1999), but a redshift was never determined for the burst. Nine months after the GRB event, no host galaxy was detected at the position of the optical transient, indicating a very faint host galaxy. Bloom et al. (1999) analyzed the light curve of the afterglow of GRB 980326 by overlaying a template of the SN 1998bw light curve at different redshifts. They found that the "GRB + supernova" model best fit the data at a redshift of $z \approx 1$ and that the rebrightening phase of the light curve was adequately described by a "supernova bump".

In this chapter and the next, we recreate Figure 1 from Bloom et al. (1999) by applying various cosmological parameters and distances to SN 1998bw data to fit a template

to GRB 980326 data. We describe our application of luminosity distance, the $K-$correction, and time dilation here. Basic concepts of cosmology are briefly explained in Appendix C, as the topic is very extensive and is often covered in a semester's worth of graduate classes (Ryden 2003).

5.1 The SN 1998bw Template

We used data of SN 1998bw to create our template (Galama et al. (1998), Patat et al. (2001)). The R-magnitude of SN 1998bw peaked on May 13.4, 1998 (JD 2450946.9), about 17 days after the detection of GRB 980425 (Galama et al. 1998). We used the spectrum from this day (Patat et al. 2001) as a standard spectrum for all later measurements (Figure 5.1). The flux at the central wavelength for the R filter (6407 Å; Bessell (2005)) was $F_\lambda = 1.003827 \times 10^{-14}\,\mathrm{erg\,s^{-1}\,cm^{-2}\,\AA^{-1}}$. We converted this to a magnitude using Equation 3.2 to find the peak R magnitude of 13.90. We held this spectrum constant in time and defined 13.90 as our "zero point". Using the photometric data of Galama et al. (1998), we determined the changes in magnitudes for the rise and decay of the supernova (Figure 5.2). The fit to the changes in magnitudes is used as the template for the redshifting of SN 1998bw.

5.2 Cosmological Parameters

We use a ΛCDM cosmological model and assume a flat universe such that $k = 0$. Using cosmological parameters from Planck Collaboration et al. (2015) we define the Hubble constant as $H_0 = 67.74 \pm 0.46\,\mathrm{km\,s^{-1}\,Mpc^{-1}}$, the matter density parameter as $\Omega_M = 0.308 \pm 0.012$, and the dark energy density parameter as $\Omega_\Lambda = 0.6911 \pm 0.0062$ (taking the curvature density parameter as $\Omega_k = 0$). The density parameters are related such that

$$\Omega_M + \Omega_\Lambda + \Omega_k = 1. \tag{5.1}$$

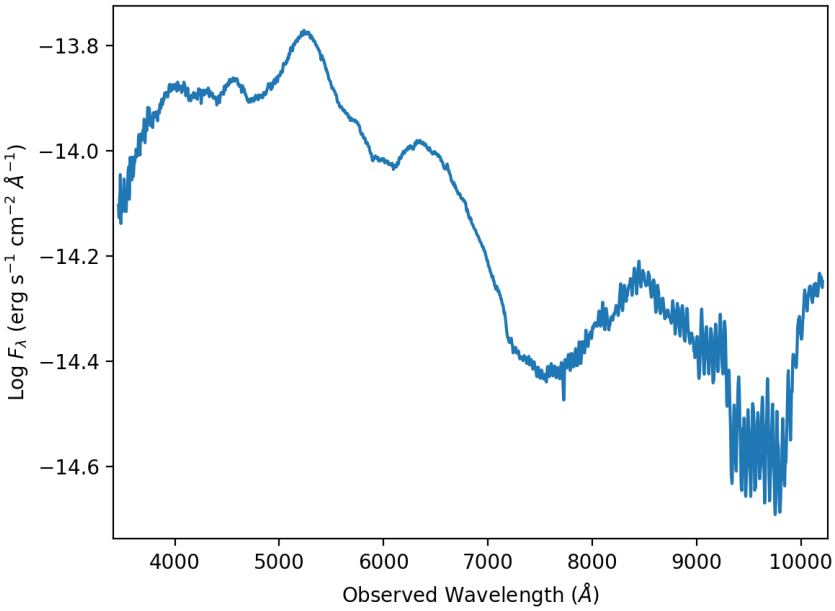

Figure 5.1: The spectrum of SN 1998bw on JD 2450946.9 (May 13, 1998). From Patat et al. (2001).

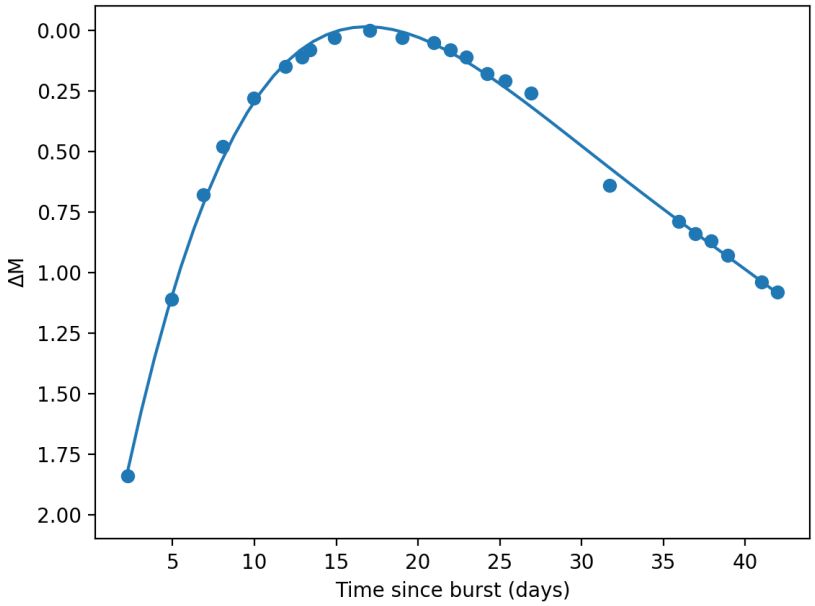

Figure 5.2: The change in magnitude of SN 1998bw with respect to its peak magnitude of 13.90.

The Hubble constant, which is the constant of proportionality between recession speed and distance in the expanding universe ($v = H_0 d$), can be used to define a characteristic scale length known as the *Hubble distance* (Hogg 2000):

$$D_H \equiv \frac{c}{H_0}, \tag{5.2}$$

with c the speed of light ($c = 3 \times 10^5 \,\mathrm{km\,s^{-1}}$). Using these cosmological parameters we can determine the effects of luminosity distance, time dilation, and the K-correction.

5.3 Redshifting using Luminosity Distance

The natural notion of distance in Euclidean space is a good approximation for objects with small redshifts but quickly falls off as redshift increases. For most redshifts, we must calculate distance using the luminosity distance formula,

$$D_L = D_H \,(1+z) \int_0^z \frac{dz'}{\left[\Omega_M (1+z)^3 + \Omega_k (1+z)^2 + \Omega_\Lambda\right]^{1/2}}, \tag{5.3}$$

described in more detail in Appendix C. This luminosity distance accounts for the expanison of the universe, unlike Euclidean distance. Flux follows an inverse-square law with distance, meaning

$$F = \frac{L}{4\pi D^2}, \tag{5.4}$$

where L is the luminosity of an object.[1] We assume that the luminosity of an object does not change with distance, allowing us to rewrite Equation 3.3 as

$$m_1 - m_2 = -2.5 \log_{10} \left(\frac{\mathrm{D}_2^2}{\mathrm{D}_1^2} \right). \tag{5.5}$$

[1] While bolometric flux scales with the inverse square of the luminosity density, flux densities (specific fluxes; i.e., energy per area time and wavelengths) require an extra factor of $(1+z)$. However, for $z \ll 1$ the scaling reduces to $1/z^2$ in either case.

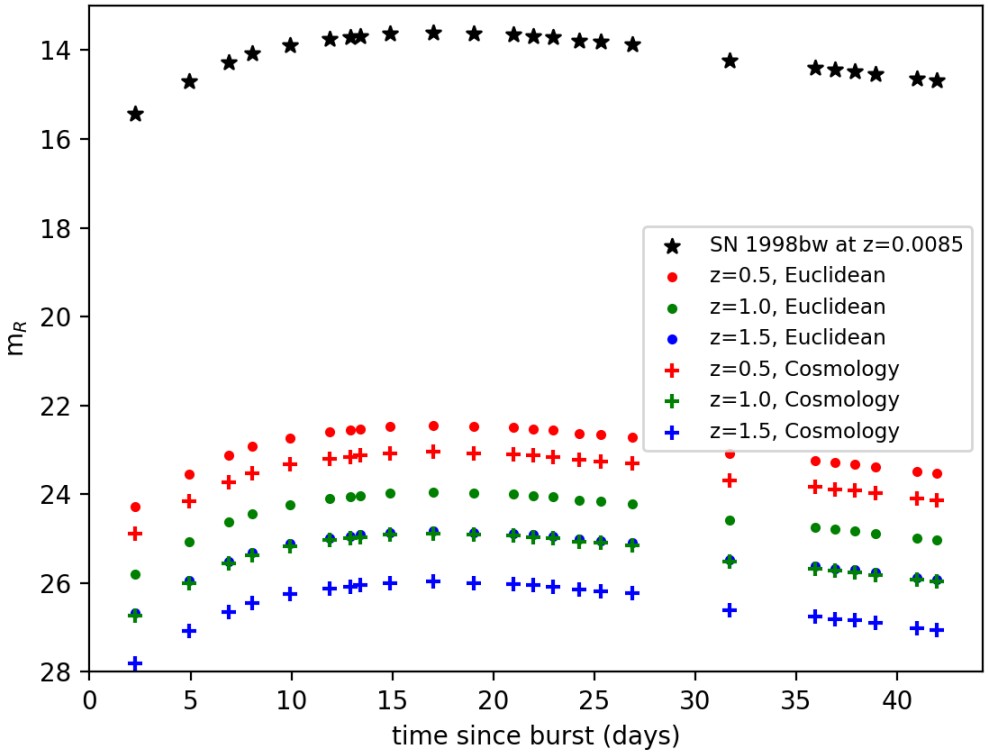

Figure 5.3: The light curve of SN 1998bw redshifted to $z = 0.5$ (red), 1.0 (green), and 1.5 (blue). Small circles indicate redshifting using the Euclidean distance and plus signs indicate redshifting using the luminosity distance. The original magnitudes are indicated by black stars.

Using Equations 5.3 and 5.5 we can shift SN 1998bw from its original redshift $z = 0.0085$ to larger redshifts tested by Bloom et al. (1999), e.g. $z = 0.5$, 1.0, and 1.5. These shifts and corresponding new magnitudes are shown in Figure 5.3.

5.4 Adjusting Timescales using Time Dilation

Expansion of the universe causes cosmological time dilation, meaning that observed light was emitted by the source at an earlier time. These times are related by a factor of

$1 + z$ such that

$$t_{rest} = \frac{t_{obs}}{(1+z)}. \tag{5.6}$$

For example, we observe that the R-band peak of GRB 980425 occurred at $t_{obs} = 17.04$ days. In the rest frame of the supernova, this peak actually occurred at

$$t_{rest} = \frac{17.04\,\text{days}}{1 + 0.0085} = 16.90\,\text{days}.$$

If SN 1998bw occurred at a redshift $z = 0.5$, then we would have seen the peak at

$$t'_{obs} = t_{rest}(1+z) = (16.90\,\text{days})(1 + 0.5) = 25.34\,\text{days}.$$

We consider time dilation effects on SN 1998bw redshifted to $z = 0.5$, 1.0, and 1.5 by first transforming into its rest frame to find t_{rest} and then transforming into the other "observed" frames. Figure 5.4 shows the new magnitudes (based on luminosity distance) and time scales of SN 1998bw.

5.5 The K-Correction

The K-correction corrects an object's magnitude (or flux) by converting a measurement from the object at redshift z into an equivalent rest-frame measurement. A photon observed with wavelength λ_o was emitted by the source with wavelength λ_e. Like the concept of time dilation, the two wavelengths are related by a factor of $1 + z$:

$$\lambda_e = \frac{\lambda_o}{1+z}. \tag{5.7}$$

We account for the K-correction by considering only this relation (a simplification of the more complicated transformation equation).

As stated in Section 5.1, the central wavelength for the R band is $\lambda_{\text{eff}} = 6407\,\text{Å}$, which corresponds to a flux of $F_\lambda = 1.003827 \times 10^{-14}\,\text{erg}\,\text{s}^{-1}\,\text{cm}^{-2}\,\text{Å}^{-1}$ in the "fixed" spec-

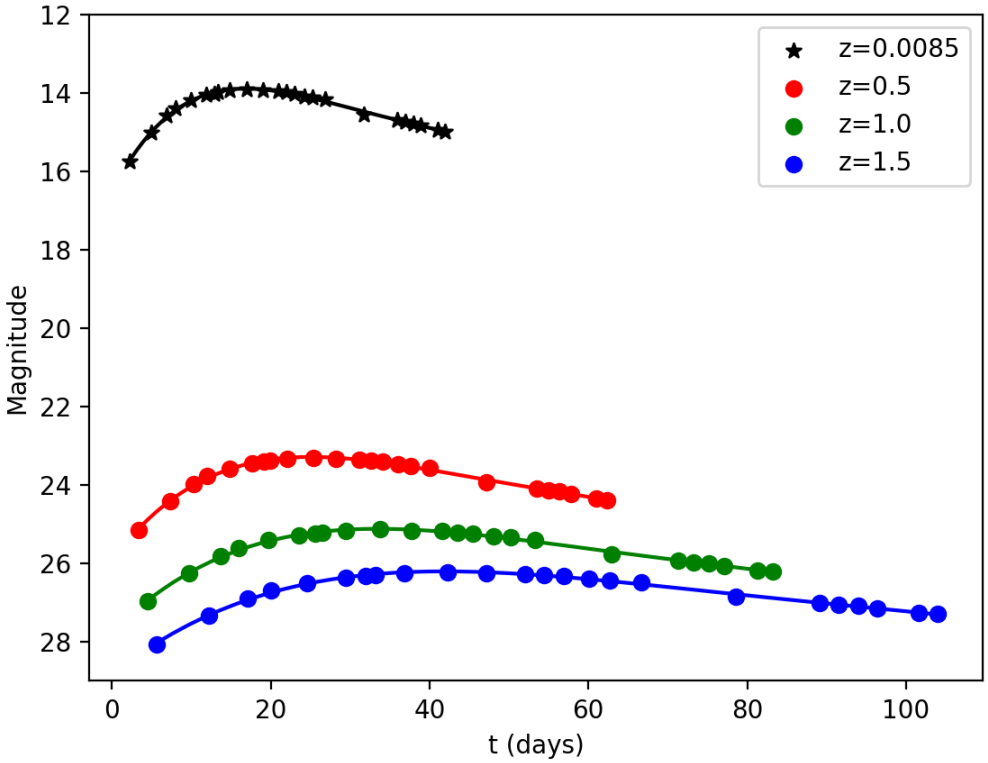

Figure 5.4: The light curve of SN 1998bw redshifted and time dilated at $z = 0.5$ (red), 1.0 (green), and 1.5 (blue). Magnitudes were calculated using luminosity distance. The original observed time scale and magnitudes are indicated by black stars.

trum of SN 1998bw. The photons we observe at 6407 Å were emitted at a wavelength

$$\lambda_e = \frac{6407\,\text{Å}}{1 + 0.0085} = 6353\,\text{Å}$$

in the rest frame of the supernova. This wavelength corresponds to a flux of $F_\lambda = 1.044349 \times 10^{-14}\,\text{erg}\,\text{s}^{-1}\,\text{cm}^{-2}\,\text{Å}^{-1}$, or a magnitude of $m_R = 13.85$. The K-correction is then

$$K = m_{R_e} - m_{R_o} = 13.85 - 13.90 = 0.05.$$

Using the fixed spectrum of SN 1998bw (Figure 5.1), we calculated the K-corrections for

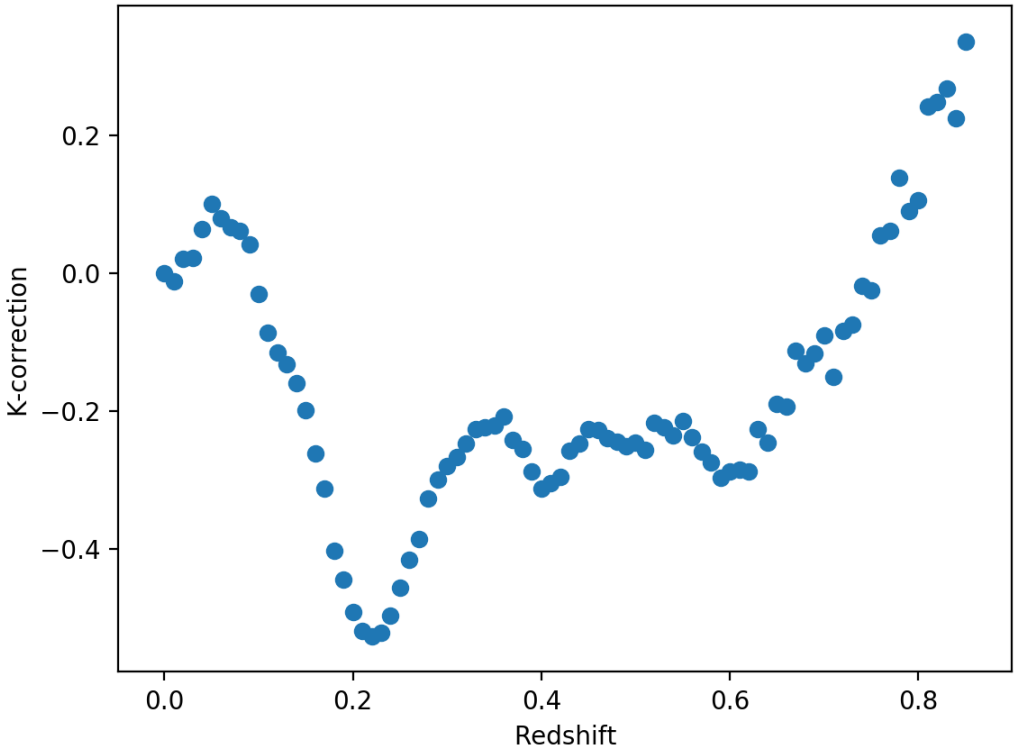

Figure 5.5: K-corrections up to redshift $z = 0.85$. These corrections are added to $m_{R_o} = 13.90$ to obtain the corrected m_{R_e}.

redshifts in the range $z = 0$ to $z = 0.85$. These K-corrections are shown in Figure 5.5. The K-corrections at $z > 0.85$ could not be determined using this method; the shortest wavelength in the spectrum is 3460 Å and gives the K-correction at $z = 0.85$. Higher redshifts correspond to $\lambda_e < 3460$ Å, for which we have a lack of data. Because of this, a K-correction was considered only for SN 1998bw redshifted to $z = 0.5$, for which $K = -0.245$. However, observations performed with small telescopes cannot usually detect objects or events past $z = 0.5$; therefore we do not need to calculate K-corrections past this limit.

Chapter 6

Applying the SN 1998bw Template

After considering luminosity distance, time-dilation, and the K-correction, we constructed a template of the SN 1998bw light curve. We applied this to GRB 980326 data to recreate Figure 1 of Bloom et al. (1999), as well as fitting data of SN 2017iuk and AT 2018cow.

6.1 Recreating the Bloom et al. (1999) Plot

We used GRB 980326 data from both Bloom et al. (1999) and Groot et al. (1998); these dates and magnitudes are included in Table 6.1. The optical transient exhibited a temporal decay that is fitted with a power law: $F_R \propto t^{-\alpha}$, where $\alpha = 2.10 \pm 0.13$ (Groot et al. 1998). The host galaxy is fainter than 27.3 magnitude, as observed almost 300 days after the detection of GRB 980326 (Bloom & Kulkarni 1998). We included this host galaxy background in our plot as well. The original Bloom et al. (1999) plot is shown in Figure 6.1a, in which SN 1998bw has been redshifted to $z = 0.50$, 0.70, 0.90, 1.10, 1.30, and 1.60. Figure 6.1b shows our template of SN 1998bw redshifted and time-dilated at redshifts $z = 0.5$, 1.0, and 1.5. We note that Bloom et al. (1999) considered time-dependent spectra to create the template whereas we kept a constant spectrum.

Date	R-magnitude	Reference
Mar 27.31	21.19 ± 0.1	Groot
Mar 27.35	21.25 ± 0.03	Bloom
Mar 27.401	21.98 ± 0.16	Groot
Mar 27.437	22.18 ± 0.16	Groot
Mar 28.016	23.66 ± 0.12	Groot
Mar 28.017	23.43 ± 0.25	Groot
Mar 28.25	23.58 ± 0.07	Bloom
Mar 28.045	23.50 ± 0.12	Groot
Mar 28.178	23.60 ± 0.12	Groot
Mar 28.25	23.69 ± 0.1	Groot
Mar 29.27	24.45 ± 0.3	Bloom
Mar 30.078	24.88 ± 0.32	Groot
Mar 30.2	25.03 ± 0.15	Groot
Mar 30.24	24.80 ± 0.15	Bloom
Mar 31.082	25.20 ± 0.23	Groot
Apr 17.25	25.34 ± 0.33	Bloom
Apr 17.3	25.5 ± 0.5	Groot
Apr 23.25	24.9 ± 0.3	Bloom
Dec 18.50	> 27.3	Bloom

Table 6.1: GRB 980326 data from Groot et al. (1998) and Bloom et al. (1999). The GRB was first detected March 26.888, 1998.

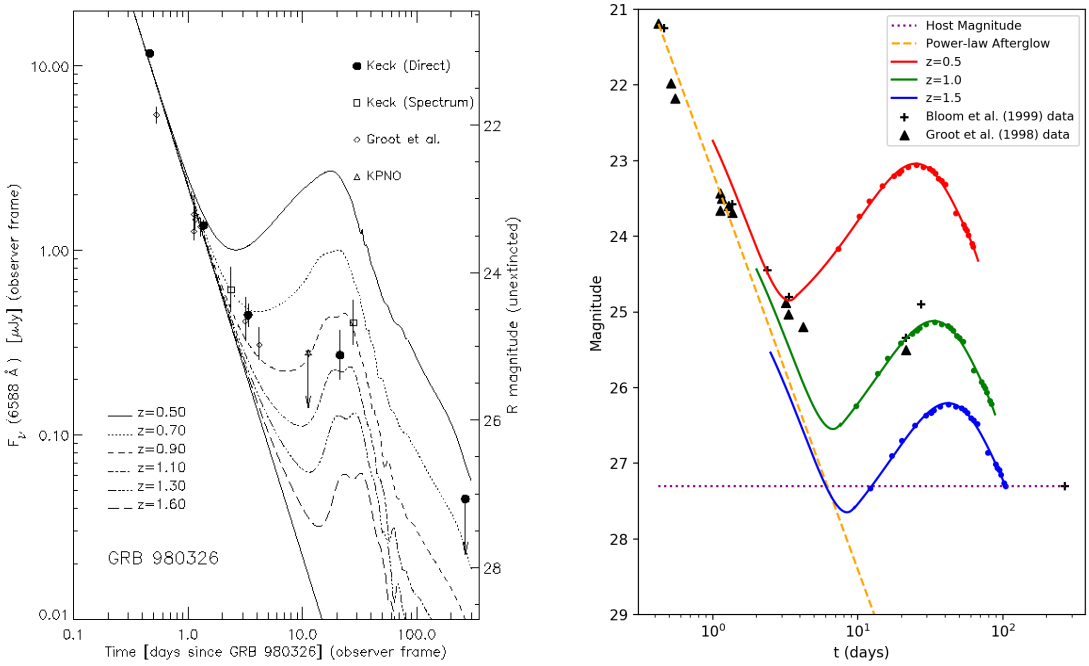

(a) GRB 980326, Bloom et al. (1999).

(b) Our plot of GRB 980326.

Figure 6.1: GRB 980326: the SN 1998bw template is shifted and time-dilated to approximate the redshift of GRB 980326.

6.2 Template-Fitting Other Data

The method of fitting data with the SN 1998bw light curve template is useful in determining the approximate redshift of GRB 980326. This template can also be used to predict when the supernova bump may emerge after the detection of a burst. We first applied our SN 1998bw template to GRB 171205A/SN 2017iuk to further examine whether this method works for other bursts as well. Although the redshift to this burst is known ($z = 0.037$), we fit the data with the template at $z = 0.03$, 0.04, and 0.06. The K-corrections at these redshifts are 0.0224, 0.0637, and 0.0796 respectively. SN 2017iuk overlaid with the SN 1998bw template is shown in Figure 6.2. The fit at $z = 0.04$ appears to describe the data best, although it predicts a brighter peak magnitude than what was observed; the fit at $z = 0.06$ also goes through several of the data points and could also be considered an "okay"

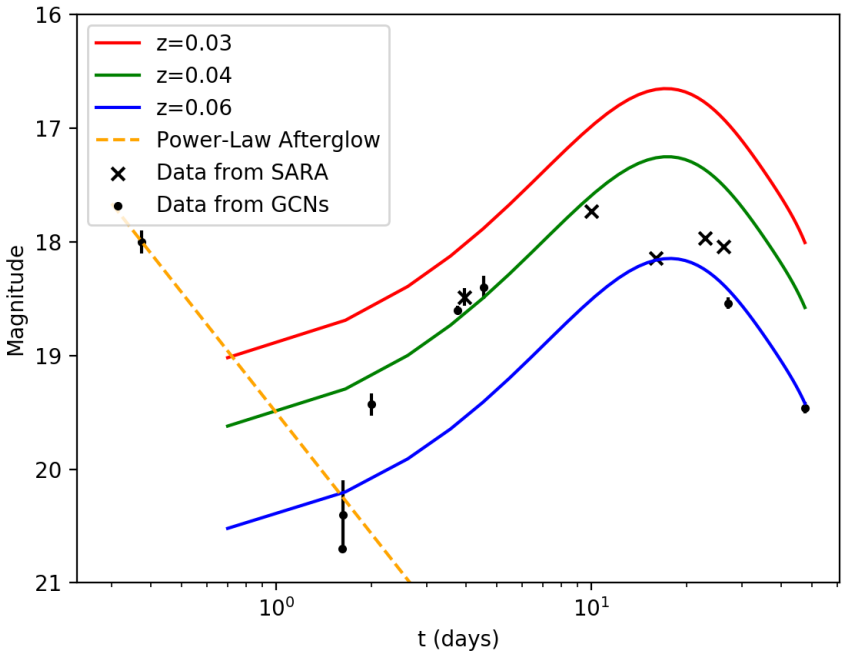

Figure 6.2: GRB 171205A / SN 2017iuk data fit with the SN 1998bw template redshifted to $z = 0.03$ (red), 0.04 (green), and 0.06 (blue). The known redshift of this burst is $z = 0.037$.

fit. If the redshift to this GRB-SN had been undetermined, we could use our template to predict a redshift of $z = 0.05 \pm 0.01$. Because neither $z = 0.04$ nor $z = 0.06$ accurately describes the data, this indicates that SN 1998bw is an imperfect template, albeit a good approximation.

We also fit the data of AT 2018cow with the SN 1998bw template. The data is fitted with a power law decay with index $\alpha = 1.39 \pm 0.02$ (Grefenstette et al. 2018) and overlaid with a supernova bump at $z = 0.014$. The K-correction at this redshift is $K = -0.0121$. If AT 2018cow had been a long duration gamma-ray burst, then we could use the template to predict when a supernova would emerge and with what magnitude. Figure 6.3 indicates that the SN would have emerged around 12 days after the detection of AT 2018cow, with a peak magnitude of about 15.0. The data on 2018-07-06 and 2018-07-17 lie close to the predicted SN bump, indicating that AT 2018cow had a supernova counterpart.

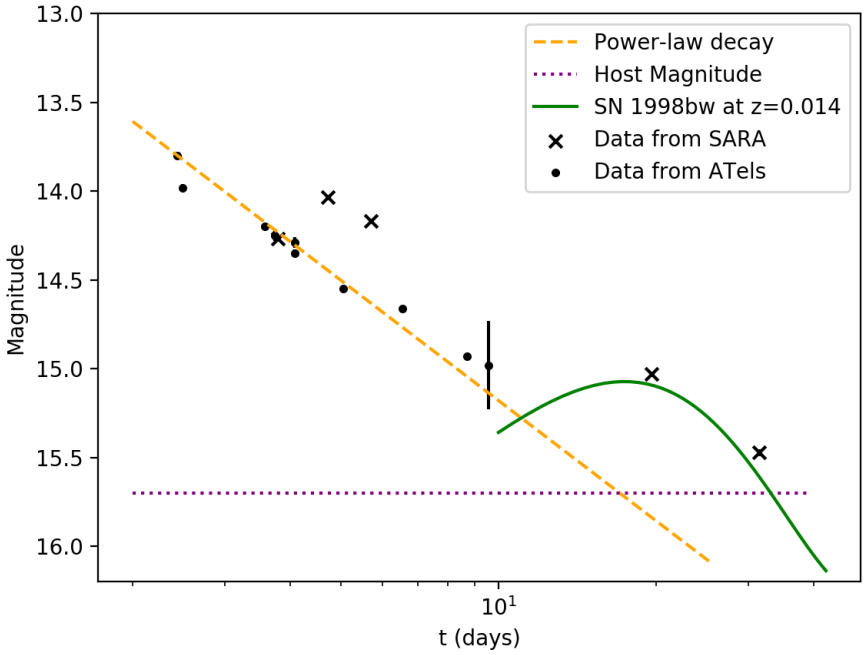

Figure 6.3: AT 2018cow data fit with the SN 1998bw template redshifted to $z = 0.014$, the known redshift of the event.

Chapter 7

Discussion and Conclusion

The connection between long gamma-ray bursts and core-collapse supernovae has been established for two decades, particularly by GRB 980425 in conjunction with SN 1998bw. Because this event was the closest GRB to date, it became one of the most scrutinized GRB-SNe in history. A plethora of data of SN 1998bw allows it to be used as a template supernova, to which other SN Ic-BL can be compared. The use of a template allows observers to approximate the redshift of a burst (if spectroscopic data are lacking) or predict when a supernova may emerge (if the redshift to a burst is known).

In this study, we observed several GRB events using three 1-m class telescopes located in both the northern and southern hemispheres as part of the SARA consortium. We modeled the light curve of GRB 171205A/SN 2017iuk with the SN 1998bw template at $z = 0.04$ as well as predicted when a supernova would emerge from AT 2018cow, assuming the event was a gamma-ray burst. We also established an upper limit of $R \sim 21$ when observing on SARA-RM. Using this upper limit we can constrain GRB observations to those at redshifts $z \leq 0.22$.

Considerable progress has been made in the field of GRB-SNe, but further studies are still needed to identify their true nature. Data on more events and independent measurements to host galaxies must be obtained to contribute to GRB-SNe population statistics. Future missions such as JWST will hopefully provide data on GRB-SNe at larger redshifts,

but only the largest ground-based telescopes can provide spectra of the most distant galaxies and SNe with sufficient resolution. Small- and medium-class telescopes are limited to observing nearby events, but are still useful in providing data on associated GRBs and SNe.

We therefore propose a simple outline for using 1-m class telescopes for observing gamma-ray bursts and supernovae. Two telescopes are needed, one in each hemisphere, with dedicated GRB-chasers. When Swift announces the detection and localization of a burst, whether through the Gamma-ray Coordinates Network or the Astronomer's Telegram, these chasers will develop an observing plan to catch the emerging supernova and observe the position of the burst for detection of the afterglow. If a redshift is determined for the burst, observers can predict the emergence of a supernova by translating and time dilating the SN 1998bw template. At low redshifts ($z \leq 0.22$), the small telescopes can be used to observe whether a supernova emerges, particularly around the predicted time frame. Although not all GRBs have an associated SN, using small telescopes to observe the skies may help to provide statistics on all nearby events. Even small telescopes can add to the ever-growing data collection of GRB-SNe.

Appendices

Appendix A Photometry and Data Reduction

A more in-depth explanation of how data reduction and photometry works.

A.1 CCD Properties and Basic Data Reduction

A CCD is a light-sensitive silicon chip divided into an array of pixels ("picture elements"), generally ranging in size of 512×512 to at least 4096×4096 individual pixels. The CCD measures how much light falls on each pixel, outputting a digital image that consists of a matrix of numbers related to the amount of light per pixel. Because CCDs vary across all telescopes, data reduction is an important step in determining the magnitudes of objects. Several properties, described below, are basic to CCD use:

- *Quantum efficiency* - The quantum efficiency (QE) is the fraction of photons falling on the CCD that are actually detected. Longer wavelength photons (i.e. red photons) can often pass through the silicon chip without being detected, thereby reducing the red sensitivity of the CCD (Howell 2000). The various absorption effects combine to define the QE of the device.

- *Gain* - The gain is the conversion between the number of electrons (e^-) recorded by the CCD and the number of digital units, or counts, that are contained within the CCD image (Howell 2000). For instance, a gain of $1.2e^-$/count means that the camera produces 1 count for every 1.2 recorded electrons.

- *Read-noise* - The read-noise is an indication of the counts produced from reading out an image after an exposure. The process of reading out the signal per pixel generates electronic noise, usually from 5 to 20 electrons per pixel (Howell 2000).

- *Bias signal* - A bias frame is a 0 s exposure used to read out any residual (the bias signal) sitting in the pixels, caused by the voltage level of the CCD camera. Bias frames are median combined into a single frame which is then subtracted from the data frames.

- *Dark signal* - A dark frame is taken with the camera shutter closed and is used to read out the number of photoelectrons in each pixel (the dark signal), which are created from the thermal properties of the CCD. Dark frames are also median combined and subtracted from the data frames.

- *Flat frame* - Because the response by each pixel varies, the CCD must be uniformly illuminated to read out the signal. When observing at night, flats should be taken with the bluest filter first (e.g. B or U) as blue light is diminshed first. Flat frames are combined per filter and the data frames are divided by the flat frames (filter-dependent) in order to normalize the response.

The basic process of data reduction can be interpreted as:

$$\text{Reduced frame} = \frac{(\text{raw object frame}) - (\text{bias frame}) - (\text{dark frame})}{(\text{flat frame})}.$$

Once the calibration images have been taken (i.e. bias frames, dark frames, and flat frames), the data images (also called "science" or "light" images) can be taken. The exposure time of a data image must be long enough to best reduce the signal-to-noise ratio (S/N), yet not so long that the pixels become saturated (generally around 65,000 counts) or that the telescope tracking fails to produce crisp images (resulting in star trails or oblong-shaped stars).

A.2 The Johnson-Cousins Photometric System

Photometric systems are characterized by the widths of their passbands and are divided into broad band ($\Delta\lambda < 1000$ Å), intermediate band ($70\text{Å} < \Delta\lambda < 400$ Å), and narrow band ($\Delta\lambda < 70$ Å). The photometric system used in this study is the Johnson-Cousins $UBVRI$ system; Figure A.1 shows the transmission windows of the $UBVRI$ filters and Table A.1 shows the peak wavelengths and widths of the system.

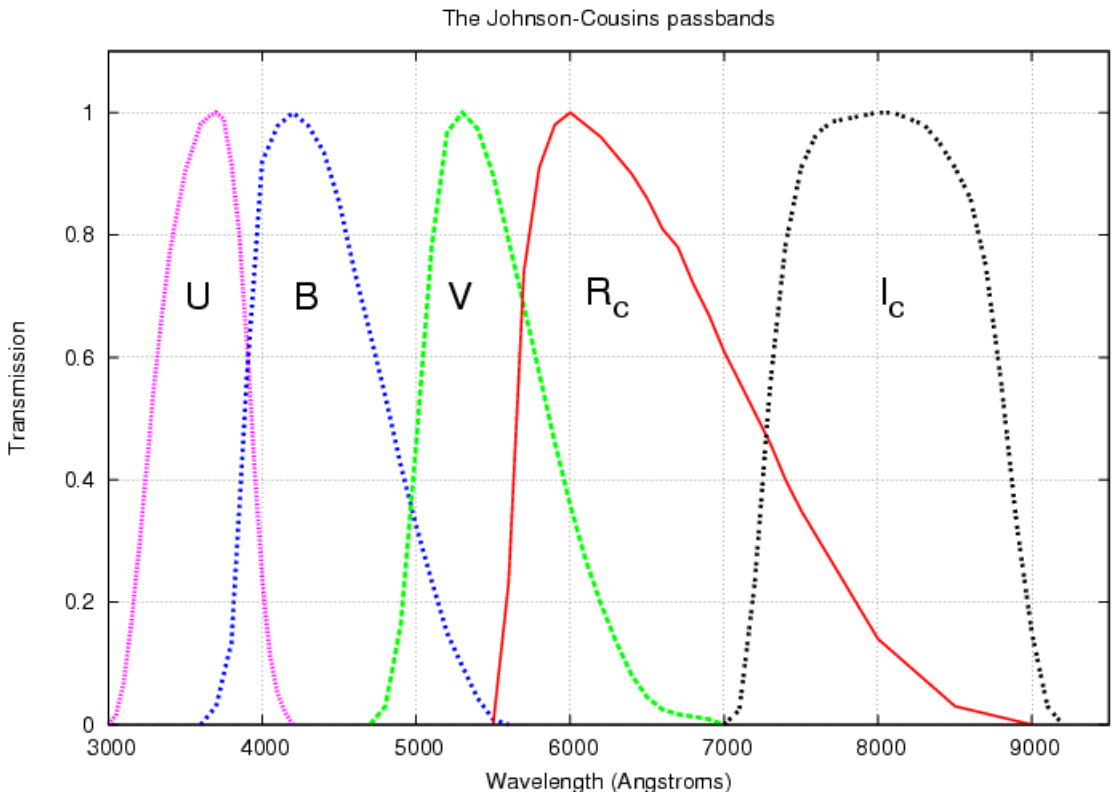

Figure A.1: Passbands of the broad-band Johnson-Cousins $UBVRI$ photometric system. From Bessell (2005).

	λ_{eff} (Å)	$\Delta\lambda$ (Å)
U	3663	650
B	4361	890
V	5448	840
R	6407	1580
I	7980	1540

Table A.1: Peak wavelengths and widths of the broad-band Johnson-Cousins $UBVRI$ photometric system. From Bessell (2005).

Site	Aperture (m)	Latitude	Longitude
Kitt Peak (KP)	0.96	+31°59′26”.1	111°35′58”.0 W
Cerro Tololo (CT)	0.6	−30°10′19”.2	70°47′57”.1 W
Roque de los Muchachos (RM)	1.0	+28°45′40”.2	17°52′41”.1 W

Table B.1: Telescopes under SARA operation and their site details. From Keel et al. (2016).

Site/Camera	Pixel scale (”)	Field (”)	Gain	Read noise (ADU)
SARA-KP ARC	0.44	899	2.3	6.0
SARA-CT FLI	0.61	622	2.0	9.7
SARA-RM Andor Ikon-L	0.34	697	1.0	6.3

Table B.2: CCD imager properties of the SARA telescopes. From Keel et al. (2016).

Appendix B SARA Consortium

The SARA consortium operates three telescopes in the 1 m class at locations in three countries (the United States, Chile, and Spain). All telescopes are operated via remote internet control through standard VCN or Radmin protocols. The SARA facilities address a broad range of scientific studies across the member institutions and allocation of nights on the telescopes is equal among partner instutions. Some flexibility in rescheduling or “trading” nights is essential, as rapid followups of transient sources, such as GRB afterglows or supernovae, are often organized on an ad hoc basis among observers.

The SARA sites are summarized in Table B.1 and the properties of the CCD systems used are summarized in Table B.2. We also include the limiting magnitudes in the B, V, and R bands for the three telescopes in Table B.3.

Site	B	V	R
Kitt Peak	20.8	20.1	20.1
Cerro Tololo	20.4	19.5	19.4
La Palma	21.4	21.6	21.1

Table B.3: Limiting magnitudes of the SARA telescopes at S/N = 10 in 10 minutes. From Keel et al. (2016).

Appendix C Cosmology Concepts

When stating the distance between two points in the Universe, one must specify which cosmological distance measure is used. In this section we will describe the formulae used to define the luminosity distance and time dilation as well as explain the concept of the K-correction.

C.1 Luminosity Distance

For very small redshifts an object's velocity is linearly proportional to its distance such that we have the relation

$$D = \frac{c}{H_0} z = D_H z, \tag{1}$$

where D_H is the Hubble distance defined in Chapter 5. This relation, sometimes referred to as the *Euclidean distance*, is only true for small redshifts (Hogg 2000). For larger redshifts we must use the *luminosity distance* to more accurately describe the distance to an object. We first define the *E-function*

$$E(z) \equiv \sqrt{\Omega_M (1+z)^3 + \Omega_k (1+z)^2 + \Omega_\Lambda}, \tag{2}$$

where z is redshift and Ω_M, Ω_k, and Ω_Λ are the three density parameters defined in Chapter 5. This function describes the evolution of the universe as it has changed from the Big Bang to today. A plot of $E(z)$ is shown in Figure C.1a. We can integrate $1/E(z)$ over the redshift interval dz, which we will call the *y-function*:

$$y(z) \equiv D_H \int_0^z \frac{dz'}{E(z')}. \tag{3}$$

This relation is also referred to as the *line-of-sight comoving distance* (Hogg 2000) and is shown in Figure C.1b. We can now relate the y-function to the luminosity distance:

$$D_L = y(z)\,(1+z) = D_H\,(1+z) \int_0^z \frac{dz'}{E(z')}. \tag{4}$$

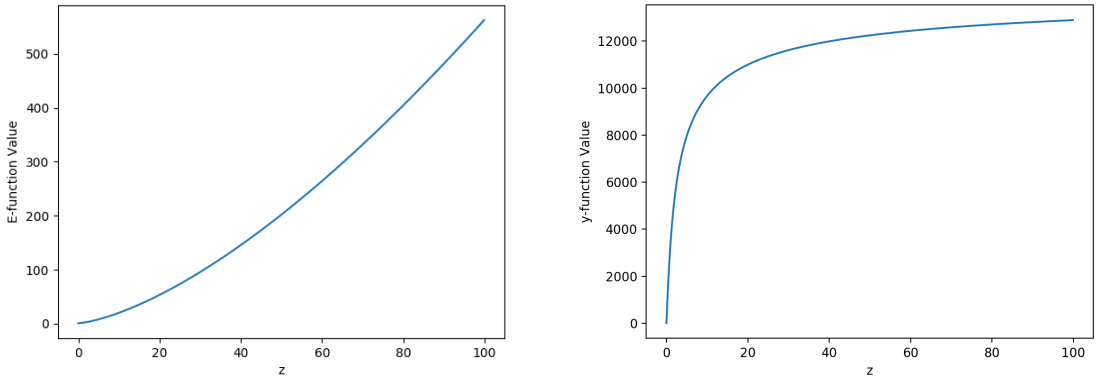

(a) $E(z)$ vs. z (b) $y(z)$ vs. z

Figure C.1: The E-function (C.1a) and the y-function (C.1b) as functions of redshift z.

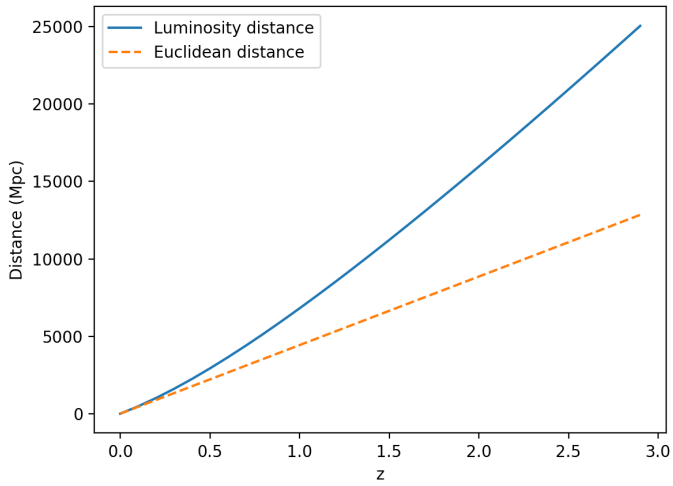

Figure C.2: Luminosity distance and Euclidean distance to a redshift $z = 3.0$.

As an example, consider an object at redshift $z = 1$. Its Euclidean distance can be calculated as $D = 4428$ Mpc, whereas its luminosity distance can be calculated as $D_L = 6802$ Mpc. This is a difference of over 2300 Mpc! Figure C.2 shows the difference between the two distance conventions to a redshift $z = 3.0$. The Euclidean distance is accurate within 1% of the luminosity distance to $z = 0.012$.

C.2 Time Dilation

In special relativity, an event as observed occurs at a later time than as it happened in the rest frame. For example, the peak of supernova light will appear to occur a few days later to observers on earth than to observers in the rest frame of the supernova. This delay of arrival time is known as cosmological time dilation and is due to the expanding universe. The duration and wavelength of emitted light from a distant object at redshift z will be dilated by a factor of $1 + z$:

$$t_{rest} = \frac{t_{obs}}{(1+z)}, \tag{5}$$

where t_{rest} is the time of the event in the rest frame and t_{obs} is the observed time of the event. This relation can also be written in terms of time intervals such that

$$\Delta t_{rest} = \frac{\Delta t_{obs}}{(1+z)}. \tag{6}$$

As a simple example, consider a supernova at $z = 1$ that appears to have a peak at 40 days to an observer. In the rest frame of the supernova, the peak actually occurred at 20 days. This cosmological expansion is evidenced by the broadening of supernovae light curves, specifically by a factor of $1 + z$ (Goldhaber et al. 2001).

C.3 K-Correction

The K-correction accounts for the fact that sources observed at different redshifts are sampled at different rest-frame wavelengths and frequencies (Hogg et al. 2002). For example, a photon observed to have a wavelength λ_o was emitted by the source at wavlength λ_e,

$$\lambda_e = \frac{\lambda_o}{1+z}. \tag{7}$$

To compute an accurate K-correction, an observer needs an accurate description of the source flux density $f_\lambda(\lambda)$, the standard-source flux densities $g^R_\lambda(\lambda)$ and $g^Q_\lambda(\lambda)$, and the bandpass functions $R(\lambda)$ and $Q(\lambda)$ (Hogg et al. 2002). Often these descriptions are not

known well. We take a simplification of the complicated transformation integral (see Equation 13 of Hogg et al. (2002)) by maintaining a constant spectrum and considering only Equation 7. The K-correction is added to the observed R magnitude, $m_{R_e} = 13.90 + K$.

Bibliography

Barthelmy, S., Cummings, J., D'Elia, V. et al. (2017), 'GRB 171205A: Swift-BAT refined analysis', *Gamma-ray Coordinates Network* **22184**.

Bessell, M. (2005), 'Standard Photometric Systems', *Annu. Rev. Astron. Astrophys.* **43**, 293–336.

Bloom, J. & Kulkarni, S. (1998), 'GRB 980326/Host Galaxy', *Gamma-ray Coordinates Network* **161**.

Bloom, J., Kulkarni, S., Djorgovski, S. et al. (1999), 'The unusual afterglow of the γ-ray burst of 26 March 1998 as evidence for a supernova connection', *Letters to Nature* **401**, 453–456.

Bloom, J. S., Frail, D. A. & Kulkarni, S. R. (2003), 'Gamma-Ray Burst Energetics and the Gamma-Ray Burst Hubble Diagram: Promises and Limitations', *ApJ* **594**, 674–683.

Bloom, J. S., Prochaska, J. X., Pooley, D. et al. (2006), 'Closing in on a Short-Hard Burst Progenitor: Constraints from Early-Time Optical Imaging and Spectroscopy of a Possible Host Galaxy of GRB 050509b', *ApJ* **638**(1), 354.

Boella, G., Butler, R., Perola, G. et al. (1997), 'BeppoSAX, the wide band mission for X-ray astronomy', *Astron. Astrophys. Sup.* **122**, 299–307.

Cano, Z., de Ugarte Postigo, A., Pozanenko, A. et al. (2014), 'A trio of gamma-ray burst supernovae: GRB 120729A, GRB 130215A/SN 2013ez, and GRB 130831A/SN 2013fu', *A&A* **568**, A19.

Cano, Z., Wang, S., Dai, Z. & Wu, X. (2017), 'The Observer's Guide to the Gamma-Ray Burst–Supernova Connection', *Advances in Astronomy* **2017**, 41.

Clocchiatti, A., Suntzeff, N., Covarrubias, R. & Candia, P. (2011), 'The Ultimate Light Curve of SN 1998bw/GRB 980425', *Astronomical Journal* **141**, 163.

Colgate, S. (1968), 'Prompt gamma rays and X rays from supernovae', *Canadian Journal of Physics* **46**, S476–S480.

de Ugarte Postigo, A., Izzo, L., Kann, D. et al. (2017), 'GRB 171205A: Detection of the emerging SN', *The Astronomer's Telegram* **11038**.

D'Elia, V., D'Ai, A., Lien, A. & Sbarufatti, B. (2017), 'GRB 171205A: Swift detection of a burst', *GRB Coordinates Network* **22177**.

Evans, P., Barthelmy, S. & Beardmore, A. (2018), 'GRB 180620A: Swift detection of a burst with an optical counterpart', *GRB Coordinates Network* **22798**.

Fishman, G. & Meegan, C. (1995), 'Gamma-Ray Bursts', *Annu. Rev. Astron. Ap.* **33**, 415–458.

Galama, T. J., Vreeswijk, P. M., van Paradijs, J. et al. (1998), 'An unusual supernova in the error box of the γ-ray burst of 25 April 1998', *Nature* **395**, 670–672.

Goldhaber, G., Groom, D., Kim, A. et al. (2001), 'Timescale stretch parameterization of Type Ia Supernova B-band light curves', *ApJ* **558**, 359–368.

Grefenstette, B., Margutti, R., Chornock, R. et al. (2018), 'Evidence for fading of the hard X-ray emission from AT2018cow', *GRB Coordinates Network* **11813**.

Greiner, J., Peimbert, M., Estaban, C. et al. (2003), 'Redshift of GRB 030329', *GRB Coordinates Network* **2020**.

Groot, P., Galama, T., Vreeswijk, P. et al. (1998), 'The Rapid Decay of the Optical Emission from GRB 980326 and its Possible Implications', *ApJ* **502**, L123–L127.

Guessoum, N., Alarayani, O., Al-Qassimi, K. et al. (2017), 'Investigating the Gamma-Ray Burst–Supernova Connection', *J. Phys.: Conf. Ser.* **869**.

Guidorzi, C., Kobayashi, S. & Mundell, C. (2018), 'GRB 180620A: LCO McDonald observations', *GRB Coordinates Network* **22803**.

Hakkila, J., Haglin, D., Roiger, R. et al. (2000), 'Properties of Gamma-Ray Burst Classes', *ApJ* **538**, 165–180.

Hartmann, D. (2010), 'A Supernova Connection', *Nature Physics* **6**, 241–243.

Hjorth, J. & Bloom, J. (2012), 'The GRB-Supernova Connection', *Cambridge Astrophysics Series* **51**, 169–190.

Hjorth, J., Sollerman, J., Møller, P. et al. (2003), 'A very energetic supernova associated with the γ-ray burst of 29 March 2003', *Nature* **423**, 847–850.

Hogg, D. (2000), Distance Measures in Cosmology. arXiv:astro-ph/9905116v4.

Hogg, D., Baldry, I., Blanton, M. & Eisenstein, D. (2002), The K Correction. arXiv:astro-ph/0210394.

Howell, S. (2000), *Handbook of CCD Astronomy*, Cambridge University Press.

Izzo, L., Kann, D., Fynbo, J. et al. (2017a), 'GRB 171205A: Likely association with low-z spiral galaxy', *GRB Coordinates Network* **22178**.

Izzo, L., Selsing, J., Japelj, J. et al. (2017b), 'GRB 171205A: VLT/X-shooter optical counterpart and spectroscopic observations', *GRB Coordinates Network* **22180**.

Keck Observatory (2016), 'W.M. Keck Observatory: NIRC2 Sensitivity'.
URL: *https://www2.keck.hawaii.edu/optics/lgsao/nirc2sens.html*

Keel, W., Oswalt, T., Mack, P. et al. (2016), 'The Remote Observatories of the Southeastern Association for Research in Astronomy (SARA)', *Astronomical Society of the Pacific* **129**.

Kitchin, C. (1998), *Astrophysical Techniques*, Institute of Physics Publishers.

Klebesadel, R., Strong, I. & Olson, R. (1973), 'Observations of Gamma-Ray Bursts of Cosmic Origin', *ApJ* **182**, 85–88.

Kouveliotou, C., Meegan, C., Fishman, G. et al. (1993), 'Identification of Two Classes of Gamma-Ray Bursts', *ApJ* **413**, 101–104.

Kulkarni, S., Frail, D., Wieringa, M. et al. (1998), 'Radio emission from the unusual supernova 1998bw and its association with the γ-ray burst of 25 April 1998', *Nature* **395**, 663–669.

Kumar, P. & Piran, T. (2000), 'Energetics and Luminosity function of Gamma-Ray Bursts', *ApJ* **535**, 152–157.

Landolt, A. (1992), 'UBVRI photometric standard stars in the magnitude range 11.5-16.0 around the celestial equator', *Astronomical Journal* **104**, 340–371.

LaPorte, S., Beardmore, A. P., Breeveld, A. et al. (2018), 'GRB 180514A: Swift detection of a burst', *GRB Coordinates Network* **22723**.

LIGO Scientific Collaboration, Virgo Collaboration, Abbott, B. et al. (2017), 'GW170817: Observation of Gravitational Waves from a Binary Neutron Star Inspiral', *Phys. Rev. Lett.* **119**, 161101.

MacFayden, A., Woosley, S. & Heger, A. (2001), 'Supernovae, Jets, and Collapsars', *ApJ* **550**(1), 410.

Marzke, R., da Costa, L., Willmer, P. & Geller, M. (1998), 'The Galaxy Luminosity Function at z $<$ 0.05: Dependence on Morphology', *ApJ* **503**, 617.

Mather, J. (2017), 'About the Webb'.
URL: *https://jwst.nasa.gov/*

Modjaz, M., Blondin, S., Kirshner, R. et al. (2014), 'Optical Spectra of 73 Stripped-Envelope Core-Collapse Supernovae', *Astron. J.* **147**, 99–116.

Modjaz, M., Liu, Y. Q., Bianco, F. B. & Graur, O. (2016), 'The Spectral SN-GRB Connection: Systematic Spectral Comparisons between Type Ic Supernovae and Broad-lined Type Ic Supernovae with and without Gamma-Ray Bursts', *ApJ* **832**(2), 108.

Monet, D., Bird, A., Canzian, B. et al. (1997), 'USNO-A2.0: A Catalog of Astrometric Standards'.
URL: *http://archive.eso.org/skycat/servers/usnoa*

Paczynski, B. (1986), 'Gamma-ray bursters at cosmological distances', *ApJ (Letters)* **308**, L43–L46.

Patat, F., Cappellaro, E., Danziger, J. et al. (2001), 'The Metamorphosis of SN 1998bw', *ApJ* **555**, 900–917.

Patat, F. & Piemonte, A. (1998), 'Supernova 1998bw in ESO 184-G82', *IAU Circ.* **6918**.

Phillips, N. (2008), 'Photometric Systems', *ALMA* .

Pian, E., Amati, L., Antonelli, L. et al. (2000), 'BeppoSAX Observations of GRB 980425: Detection of the Prompt Event and Monitoring of the Error Box', *ApJ* **536**, 778–787.

Planck Collaboration, Ade, P., Aghanim, N. et al. (2015), 'Planck 2015 results. XIII. Cosmological parameters', *A&A* **594**, A13.

Price, P. & Peterson, B. (2003), 'GRB 030329: Optical afterglow candidate', *GRB Coordinates Network* **1987**.

Rivera Sandoval, L. & Maccarone, T. (2018), 'Swift follow-up observations of the optical transient AT2018cow/ATLAS18qqn', *The Astronomer's Telegram* **11737**.

Ryden, B. (2003), *Introduction to Cosmology*, Addison Wesley.

Schmidt, M. (2001), 'Luminosity Function of Gamma-Ray Bursts Derived without Benefit of Redshifts', *ApJ* **552**, 36–41.

Schweyer, T. & Schady, P. (2018), 'GROND observations of GRB 180620A', *GRB Coordinates Network* **22818**.

Smartt, S., Clark, P., Smith, K. et al. (2018), 'ATLAS18qqn (AT2018cow) - a bright transient spatially coincident with CGCG 137-068 (60 Mpc)', *The Astronomer's Telegram* **11727**.

Soderberg, A., Nakar, E., Berger, E. & Kulkarni, S. (2006), 'Late-Time Radio Observations of 68 Type IBC Supernovae: Strong Constraints on Off-Axis Gamma-Ray Bursts', *ApJ* **638**(2).

Sollerman, J., Holland, S. T., Challis, P. et al. (2002), 'Supernova 1998bw - the final phases', *A&A* **386**, 944–956.

Sterken, C. & Manfroid, J. (1992), *Astronomical Photometry: A Guide*, Kluwer Academic Publishers.

Tinney, C., Stathakis, R., Cannon, R. & Galama, T. (1998), 'GRB 980425', *IAU Circ.* **6896**.

Woosley, S. & Bloom, J. (2006), 'The Supernova Gamma-Ray Burst Connection', *Annu. Rev. Astron. Ap.* **44**, 507–556.

Woosley, S. E. & Heger, A. (2006), 'The Progenitor Stars of Gamma-Ray Bursts', *ApJ* **637**(2), 914.

Zeh, A., Klose, S. & Hartmann, D. (2004), 'Evidence for Supernova light in all Gamma-Ray Burst afterglows', *22nd Texas Symposium on Relativistic Astrophysics* pp. 617–620.

Zwicky, F. & Herzog, F. (1963), Catalogue of Galaxies and of Clusters of Galaxies, Technical report, California Institute of Technology.